Electronic Supplementary Material (ESI) for Green Chemistry.

Supporting Information

Achieving Superior Methanol Oxidation Electrocatalytic Performance by Surface Reconstruction of PtNi Nanoalloys during Acid Etching Process

Xu Chen, Jinyu Zhao, Jie Lian, Xiaomin Wang*

College of Materials Science and Engineering, Taiyuan University of Technology, 030024, PR China

E-mail address: wangxiaomin@tyut.edu.cn (X. Wang)

The apparent activation energy (Ea) can be obtained from the fitting slope of Arrhenius diagram (ln j vs. 1/T), according to the following equation:

$$I = Ae - \frac{E_a}{RT} \quad (1)$$

where A is the pre-exponential, R represents gas constant, and T is the reaction temperature.

The potential measured with a SCE electrode can be transferred according to the following equation:

$$E_{(RHE)} = E_{(SCE)} + 0.2415\ V + 0.05916 \times pH \quad (2)$$

The hydrogen desorption region was used to integrate with the positive-going potential scan to obtain electrochemically active surface areas (ECSA) evaluated by the following equation:

$$ECSA = \frac{S}{MC\nu} \quad (3)$$

where S is the integral area of the hydrogen region obtained from the CV curve. M is the Pt loading on the surface of the electrode, and C is the H adsorption constant of Pt single crystal (0.21 mC cm^{-2}), ν is the scanning speed (50 mV s^{-1}).

The mass activity and specific activity obtained from the following equations:

$$J_{k\ mass} = \frac{J_k S}{M_{Pt}} \quad (4)$$

$$J_{k\ specific} = \frac{J_k S}{ECSA\ M_{Pt}} \quad (5)$$

J_k is the peak current density of catalysts obtained from the CV curves in 0.5 M H_2SO_4 containing 1 M CH_3OH solution. S is the geometric area of the GCE. M_{Pt} is the

Pt loading on the surface of the electrode.

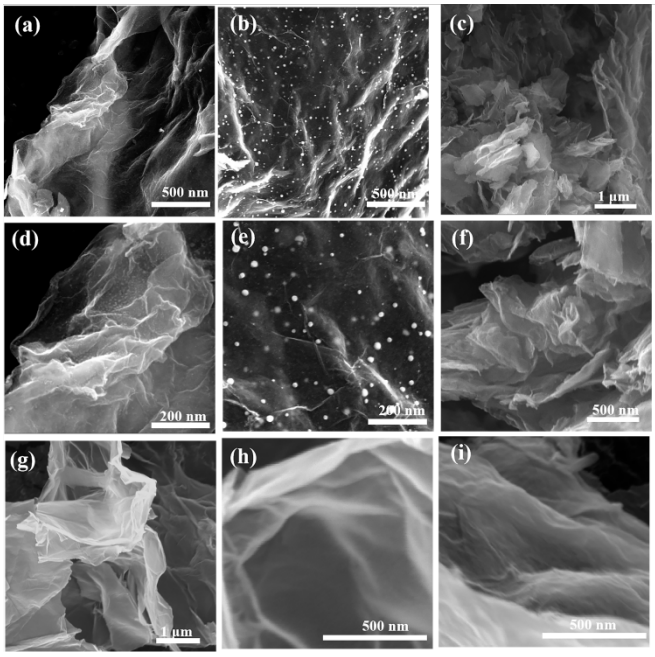

Fig. S1 The SEM images of (a, d) $Pt_{1.5}Ni$-NGA, (b, e) $PtNi_3$-NGA (c, f) Pt-NGA, (g, h) rGO and (i) $PtNi_3$-NGA precursor.

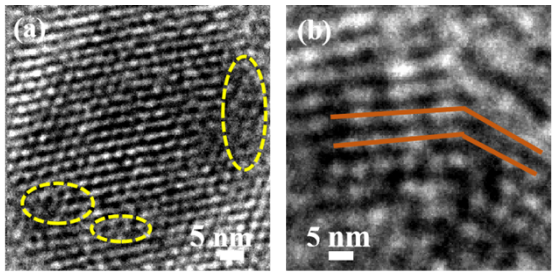

Fig. S2 HRTEM images of $Pt_{1.5}Ni$-NGA catalysts.

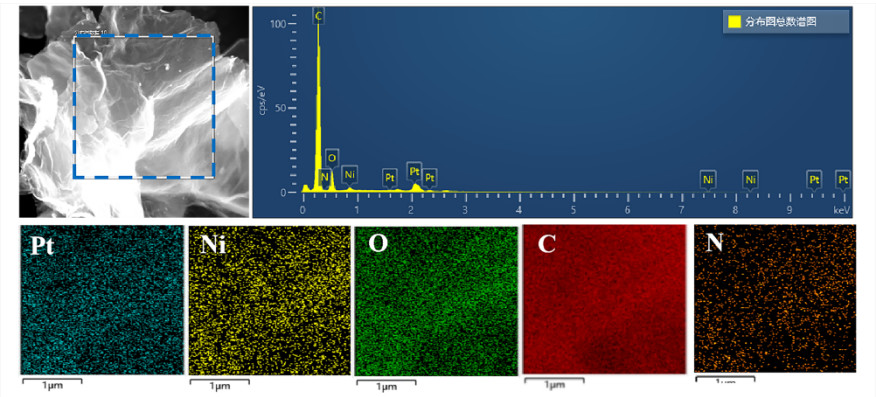

Fig. S3 SEM and its corresponding EDS mapping images of $Pt_{1.5}Ni$-NGA catalyst.

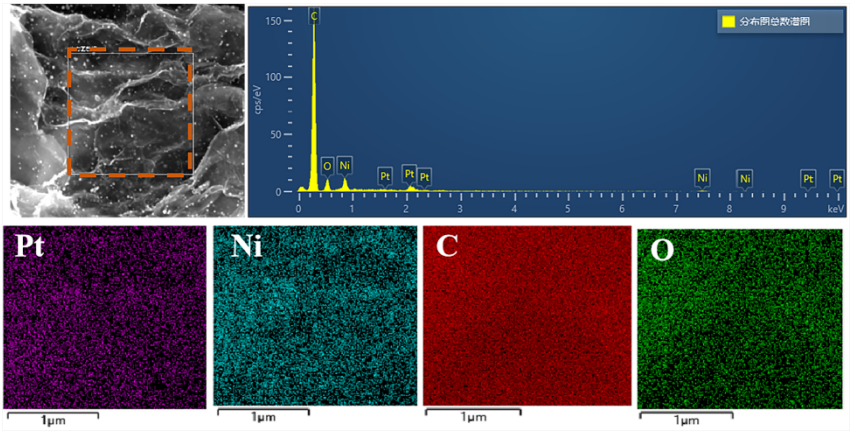

Fig. S4 SEM and its corresponding EDS elemental mapping images of the $PtNi_3$-NGA catalyst.

Table S1 ICP results of the obtained samples.

Sample	Pt (wt%)	Pt/Ni atomic ratio
Pt_3Ni-NGA	13.9	3:1
Pt_2Ni-NGA	13.5	1.98:1
PtNi-NGA	12.5	1:1
$PtNi_2$-NGA	10.8	1:2
$PtNi_3$-NGA	15.5	1:3.1

$PtNi_4$-NGA	8.4	1:4
$Pt_{1.5}Ni$-NGA	9.5	1.5:1
Pt-NGA	23.5	
$PtNi_3$-rGO	21	/
Pt/C	20	

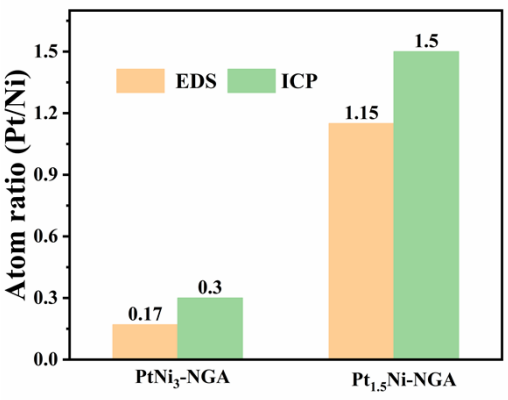

Fig. S5 Pt/Ni atom ratio characterized by EDS and ICP-OES.

Table S2 The Percentage of elements from EDS elemental mapping.

Samples	**Elements (Wt %)**					
	Pt	**Ni**	**O**	**C**	**N**	**Pt/Ni (at%)**
$Pt_{1.5}Ni$-NGA	7.73	2.04	11.04	78.53	0.67	1.15
$PtNi_3$-NGA	4.11	7.45	6.37	82.06	0	0.17

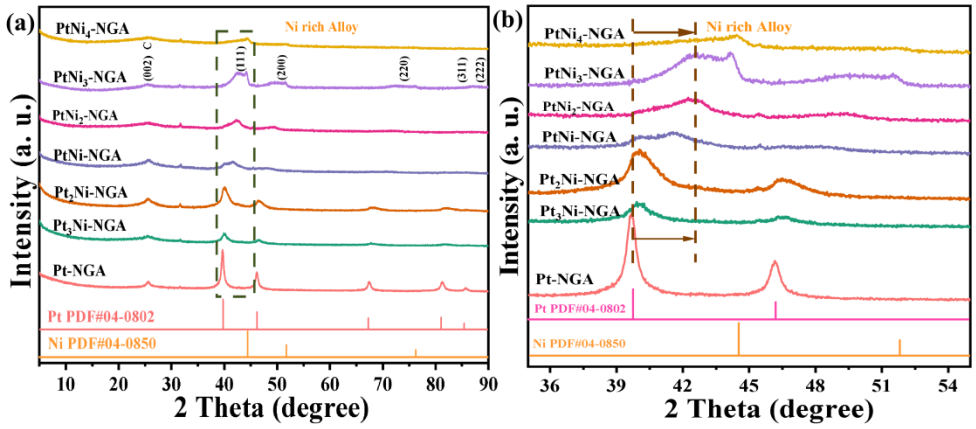

Fig. S6 (a) XRD patterns and (b) the corresponding magnified views of Pt_xNi_y-NGA samples with different Ni contents.

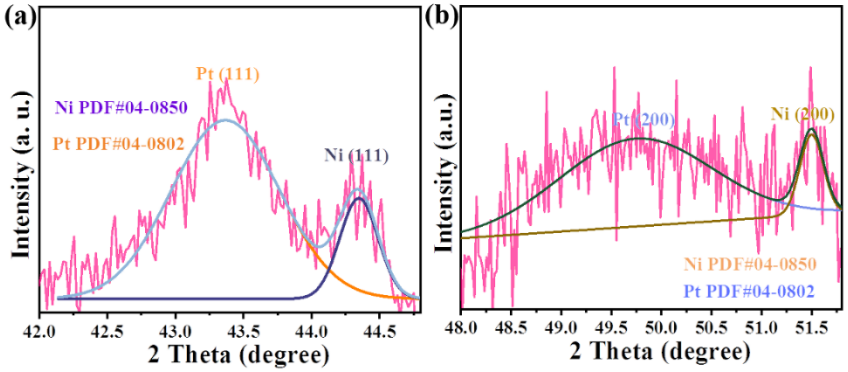

Fig. S7 The deconvolution of the broad peaks (a) at 42-45° and (b) 48-52°.

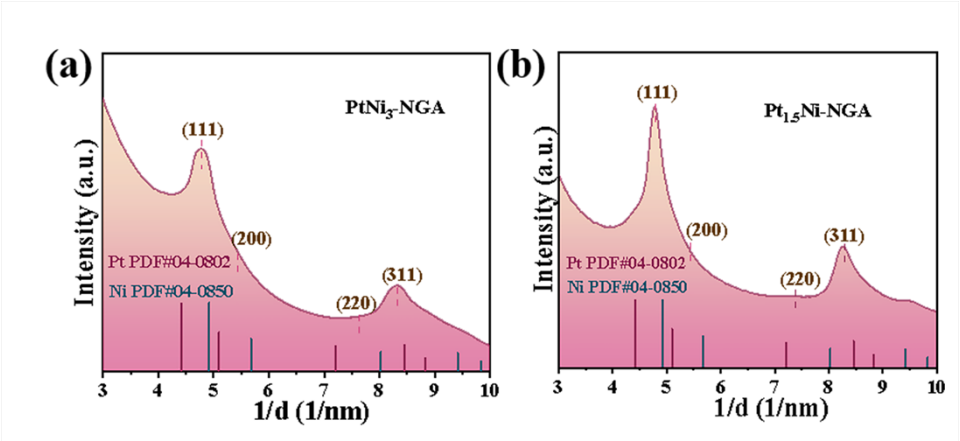

Fig. S8 SAED diffraction speckle calibration of (a) $PtNi_3$-NGA and (b) $Pt_{1.5}$Ni-NGA.

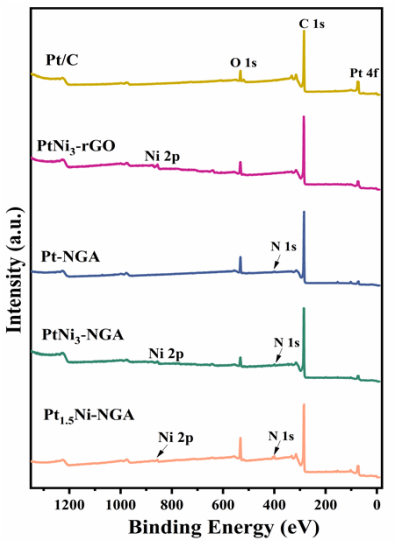

Fig. S9 XPS survey spectra of $Pt_{1.5}Ni$-NGA, $PtNi_3$-NGA, Pt-NGA, $PtNi_3$-rGO and Pt/C catalysts.

Table S3 The Percentage of elements obtained from XPS.

Samples	Elements (Atom %)				
	Pt	Ni	C	N	Pt/Ni
$Pt_{1.5}Ni$-NGA	0.42	0.31	96.11	3.17	1.35
$PtNi_3$-NGA	0.60	1.12	96.17	2.11	0.54
Pt-NGA	0.44	-	97.56	2	-
$PtNi_3$-rGO	0.97	1.99	97.04	-	0.49
Pt/C	2.32	-	97.68	-	-

Table S4 Binding energies and surface components for Pt 4f core level region of all catalysts.

Catalysts	Pt^0	Pt^{2+}
	Binding energy (eV)	**Binding energy (eV)**
$Pt_{1.5}Ni$-NGA	71.92	73.63
	75.23	76.93
$PtNi_3$-NGA	71.65	73.18
	74.98	76.51
Pt-NGA	71.11	73.03
	74.44	76.01
$PtNi_3$-rGO	71.70	73.50
	75.03	76.83
Pt/C	71.20	72.40
	74.53	75.73

Table S5 Contents of nitrogen based on N 1s high-resolution XPS analysis for different samples**.**

Sample	Configuration of nitrogen (%)			
	Pyridinic N (%)	**Pyrrolic N (%)**	**Graphitic N (%)**	**Oxidized N (%)**
$Pt_{1.5}Ni$-NGA	32.7	14.0	23.7	29.6
$PtNi_3$-NGA	26.6	43.7	20.3	9.4
Pt-NGA	38.6	22.2	36.3	2.9

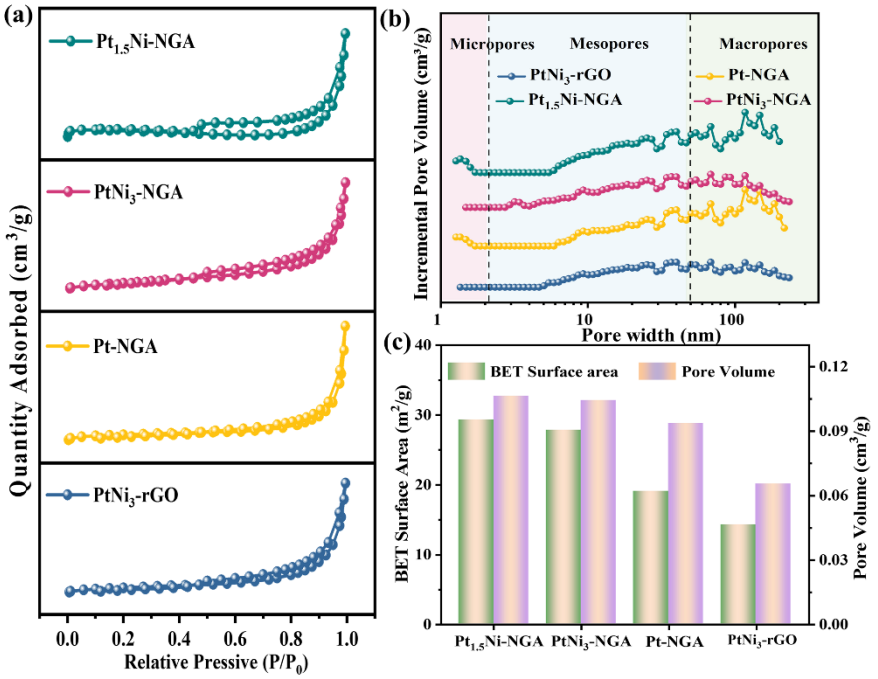

Fig. S10 (a) N_2 adsorption/desorption isotherms, (b) corresponding pore distribution, (c) the BET and the pore volume distribution histograms of prepared catalysts.

Table S6 The BET and total pore volume of all samples.

Samples	S_{BET} (m^2/g)	V_t (cm^3/g)
$Pt_{1.5}Ni$-NGA	29.2779	0.106306
$PtNi_3$-NGA	27.8300	0.104293
Pt-NGA	19.0169	0.093555
$PtNi_3$-rGO	14.2000	0.065207

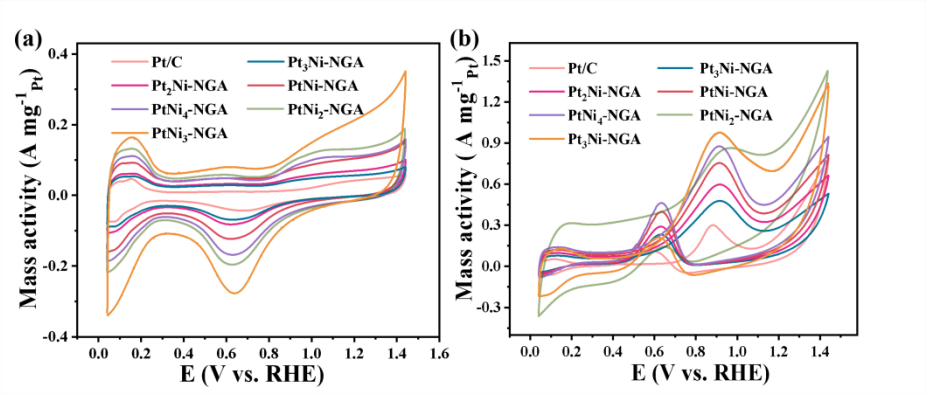

Fig. S11 Catalytic activity characterizations. (a) CV curves in 0.5 M H_2SO_4 solution at a scan rate of 50 mV s^{-1} and (b) CV curves in 0.5 M H_2SO_4 + 1.0 M CH_3OH solution at a scan rate of 50 mV s^{-1}.

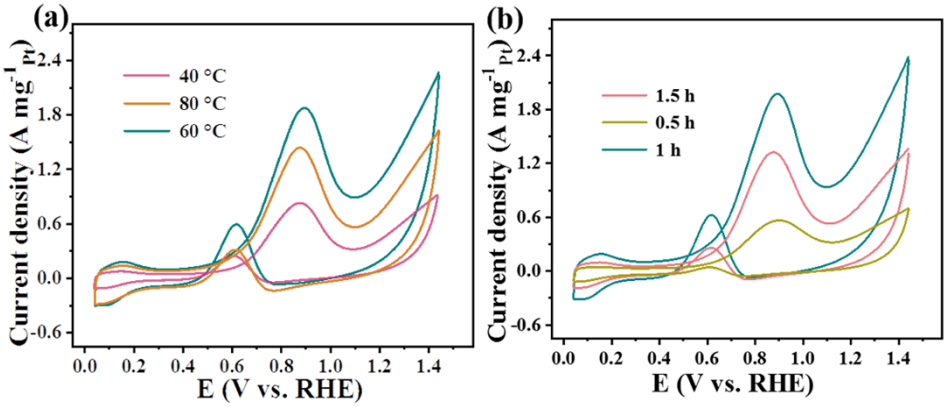

Fig. S12 CV curves of $PtNi_3$-NGA acid etching (a) for 1 h from 40 °C to 80 °C, (b) at 60 °C for 0.5-1.5 h in 0.5 M H_2SO_4 + 1.0 M CH_3OH.

Table S7 The comparison of ESCA, Mass activity and Specific activity of all samples.

Sample	ESCA ($m^2 g^{-1}$)	Mass activity ($A mg^{-1}$)	Specific activity ($mA cm^{-2}$)
$Pt_{1.5}Ni$-NGA	205.10	1.88	0.93
$PtNi_3$-NGA	155.79	0.98	0.92
Pt-NGA	78.62	0.79	0.81
$PtNi_3$-rGO	59.93	0.58	0.97
Pt/C	50.78	0.30	0.59

Table S8 Comparison of the MOR performance for recently reported Pt-based electrocatalysts in acid electrolytes.

Catalysts	Mass activity ($A mg_{Pt}^{-1}$)	Electrolyte	References
$Pt_{1.5}Ni$-NGA	1.88	0.5 M H_2SO_4 + 1.0 M CH_3OH	This work
$Pd_{59}Fe_{27}Pt_{14}$	1.61	0.1 M $HClO_4$ +0.5 M CH_3OH	[1]
PtNiNF-NGA	1.65	0.1 M $HClO_4$ +1.0 M CH_3OH	[2]
PtFe (1:2) @a-FeO_x/NC-C	1.48	0.5 M H_2SO_4 + 1.0 M CH_3OH	[3]
CuNi@Pt-Cu nano-octahedra	0.99	0.1 M $HClO_4$ +1.0 M CH_3OH	[4]
PtFe@PtRuFe	0.69	0.1 M $HClO_4$ +0.5 M CH_3OH	[5]
d-Pt@Ru dodecahedra	0.80	0.5 M H_2SO_4 + 1.0 M CH_3OH	[6]
ae-$P_3Te_6Co_2$ nanorods	1.47	0.1 M $HClO_4$ +0.5 M CH_3OH	[7]
PtCo nanocrosses	0.69	0.5 M H_2SO_4 + 1.0 M CH_3OH	[8]
Ir-Pt-Cu	1.04	0.1 M $HClO_4$ +0.5 M CH_3OH	[9]
0.5%Sn/Pt_3Mn	0.65	0.5 M H_2SO_4 + 2.0 M CH_3OH	[10]
Hollow PtCu nanotube	1.33	0.5 M H_2SO_4 + 1.0 M CH_3OH	[11]

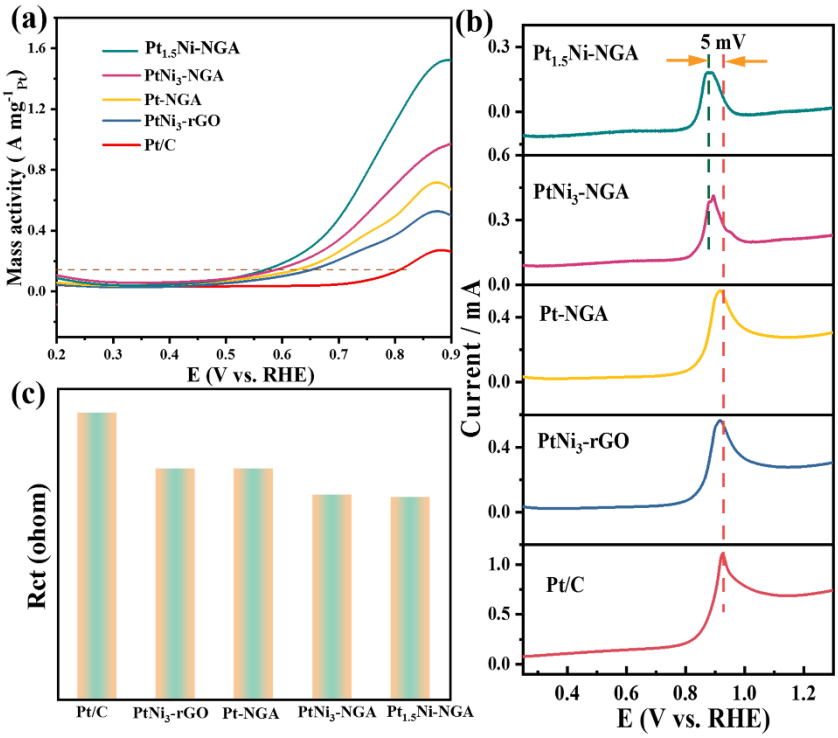

Fig. S13 (a) LSV curves of all catalysts in 0.5 M H_2SO_4 + 1.0 M CH_3OH at a sweeping rate of 5 mV s^{-1}. (b) CO-stripping curves obtained in 0.5 M H_2SO_4 at a scan rate of 50 mV s^{-1}. (c) Histograms of Rct derived from the electrochemical impedance plots.

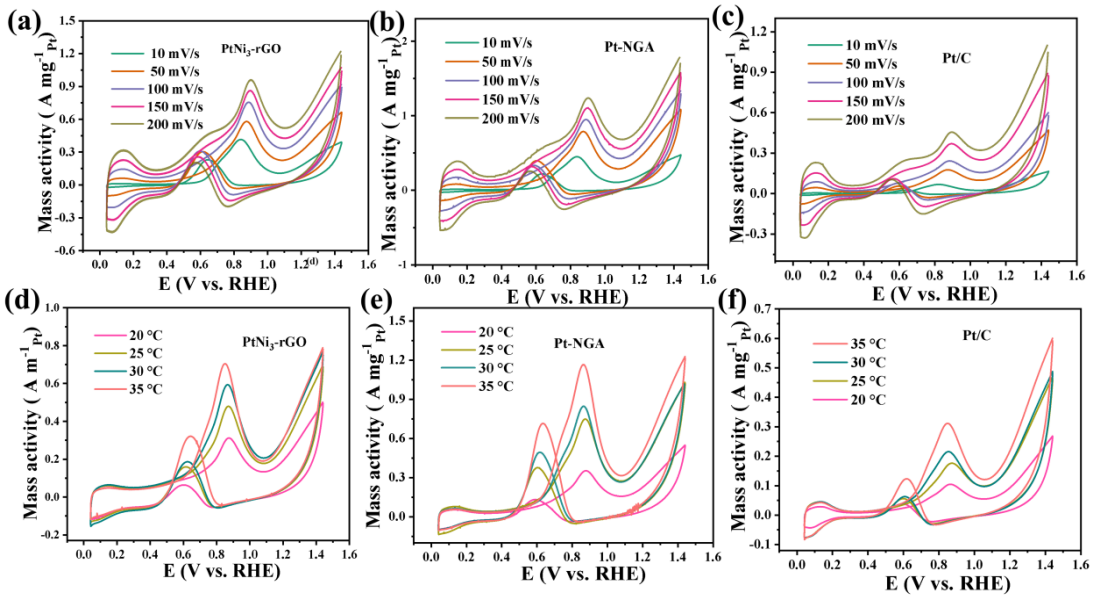

Fig. S14 (a-c) MOR CV curves at various scan rate of $PtNi_3$-rGO, Pt-NGA and Pt/C. (d-f) MOR

CV curves of $PtNi_3$-rGO, Pt-NGA and Pt/C catalysts at 50 mV/s from 20 °C to 35 °C in 0.5 M H_2SO_4 + 1.0 M CH_3OH.

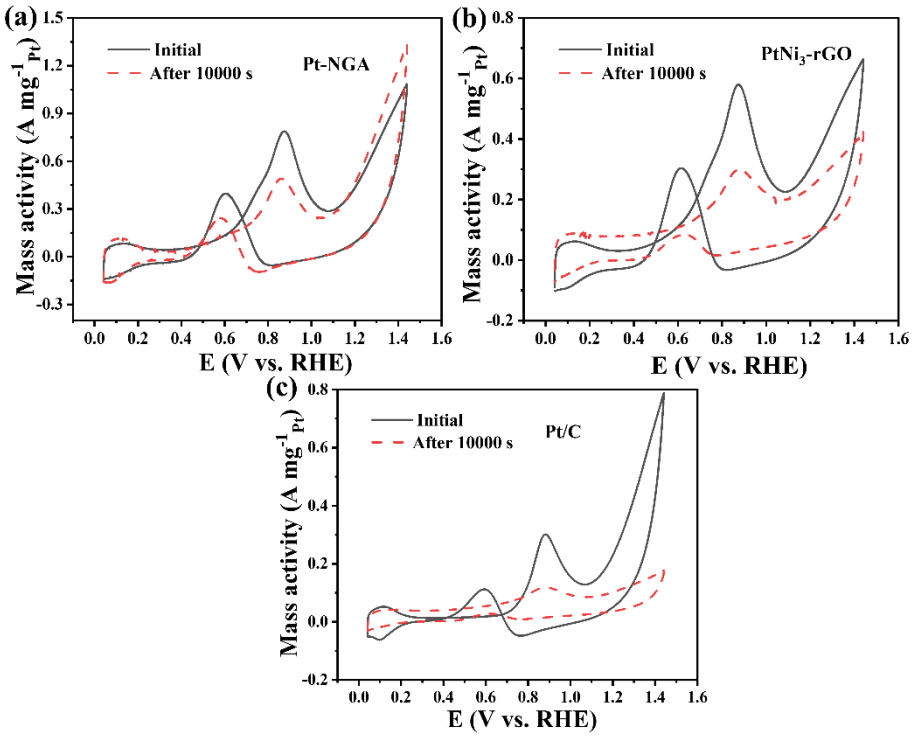

Fig. S15 MOR CV curves of (a) Pt-NGA, (b) $PtNi_3$-rGO and (c) Pt/C, recorded before (solid line) and after (dotted line) 10000 s i-t test.

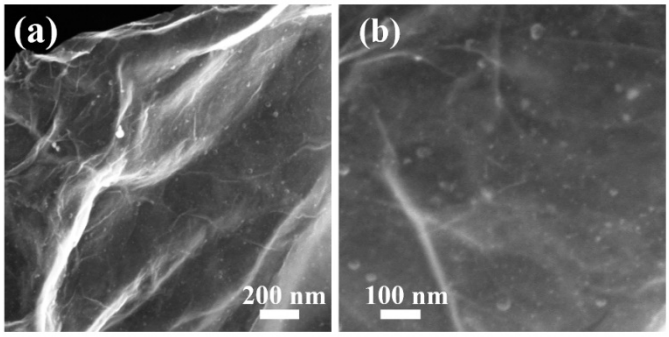

Fig. S16 SEM images of $Pt_{1.5}$Ni-NGA catalyst after 10000 s i-t test.

References

[1] Luo, X., C. Liu, X. Wang, Q. Shao, Y. Pi, T. Zhu, Y. Li, and X. Huang. "Spin Regulation on 2D Pd-Fe-Pt Nanomeshes Promotes Fuel Electrooxidations." Nano Lett, 20, 2020, 1967-73.

[2] Yang, J., R. Hubner, J. Zhang, H. Wan, Y. Zheng, H. Wang, H. Qi, et al. "A Robust PtNi Nanoframe/N-Doped Graphene Aerogel Electrocatalyst with Both High Activity and Stability." Angew Chem Int Ed Engl, 60, 17, 2021, 9590-97.

[3] Zhao, W., L. Ma, M. Gan, X. Li, Y. Zhang, X. Hua, and L. Wang. "Engineering Intermetallic-Metal Oxide Interface with Low Platinum Loading for Efficient Methanol Electrooxidation." J Colloid Interface Sci, 604, 2021, 52-60.

[4] Li, C., X. Chen, L. Zhang, S. Yan, A. Sharma, B. Zhao, A. Kumbhar, G. Zhou, and J. Fang. "Synthesis of Core@Shell Cu-Ni@Pt-Cu Nano-Octahedra and Their Improved Mor Activity." Angew Chem Int Ed Engl, 60, 14, 2021, 7675-80.

[5] Wang, Qingmei, Siguo Chen, Pan Li, Shumaila Ibraheem, Jia Li, Jianghai Deng, and Zidong Wei. "Surface Ru Enriched Structurally Ordered Intermetallic PtFe@PtRuFe Core-Shell Nanostructure Boosts Methanol Oxidation Reaction Catalysis." Applied Catalysis B: Environmental, 252, 2019, 120-27.

[6] Bai, X., J. Geng, S. Zhao, H. Li, and F. Li. "Tunable Hollow Pt@Ru Dodecahedra Via Galvanic Replacement for Efficient Methanol Oxidation." ACS Appl Mater Interfaces, 12, 20, 2020, 23046-50.

[7] Li, Jie, Cheng Wang, Hongyuan Shang, Yuan Wang, Huaming You, Hui Xu, and Yukou Du. "Metal-Modified $PtTe_2$ Nanorods: Surface Reconstruction for Efficient

Methanol Oxidation Electrocatalysis." Chemical Engineering Journal, 424, 2021.

[8] Li, Zhijuan, Xian Jiang, Xiaoru Wang, Jinrui Hu, Yuanyuan Liu, Gengtao Fu, and Yawen Tang. "Concave PtCo Nanocrosses for Methanol Oxidation Reaction." Applied Catalysis B: Environmental, 277 2020.

[9] Peng, K., W. Zhang, N. Bhuvanendran, Q. Ma, Q. Xu, L. Xing, L. Khotseng, and H. Su. "Pt-Based (Zn, Cu) Nanodendrites with Enhanced Catalytic Efficiency and Durability toward Methanol Electro-Oxidation Via Trace Ir-Doping Engineering." J Colloid Interface Sci, 598, 2021, 126-35.

[10] Li, Yunrui, Yao Wang, Shuna Li, Mingxuan Li, Yujie Liu, Xu Fang, Xiaoping Dai, and Xin Zhang. "Pt_3Mn Alloy Nanostructure with High-Index Facets by Sn Doping Modified for Highly Catalytic Active Electro-Oxidation Reactions." Journal of Catalysis, 395, 2021, 282-92.

[11] Xu, F., S. Cai, B. Lin, L. Yang, H. Le, and S. Mu. "Geometric Engineering of Porous PtCu Nanotubes with Ultrahigh Methanol Oxidation and Oxygen Reduction Capability." Small, 2022, e2107387.